Applied Catalysis B: Environmental 256 (2019) 117866

Contents lists available at ScienceDirect

Applied Catalysis B: Environmental

journal homepage: www.elsevier.com/locate/apcatb

Inactivation of harmful cyanobacteria by Ag/AgCl@ZIF-8 coating under visible light: Efficiency and its mechanisms

Gongduan Fan[a,b,*], Yifan You[a], Bo Wang[c], Shimin Wu[d], Zhi Zhang[e], Xiaomei Zheng[a], Minchen Bao[a], Jiajun Zhan[a]

[a] College of Civil Engineering, Fuzhou University, 350116 Fujian, China
[b] State Key Laboratory of Photocatalysis on Energy and Environment, Fuzhou University, 350002 Fujian, China
[c] School of Urban Planning and Design, Shenzhen Graduate School, Peking University, 518055 Guangdong, China
[d] IER Environmental Protection Engineering Technology Co., Ltd., 518071 Guangdong, China
[e] College of Environment and Ecology, Chongqing University, 400044 Chongqing, China

ARTICLE INFO

Keywords:
Photocatalysis
Microcystis aeruginosa
Ag/AgCl@ZIF-8
Coating
Visible light

ABSTRACT

A novel floating photocatalyst was prepared by depositing Ag/AgCl@ZIF-8 on a sodium dodecyl benzene sulfonate modified sponge with a simple dip-coating method and was employed for the inactivation of harmful cyanobacteria for the first time. The effect of coated sponge on *Microcystis aeruginosa* under visible light was investigated and a possible mechanism was proposed. The results showed that the synthesized photocatalyst exhibited outstanding performance with a high removal efficiency of chlorophyll *a* reaching 98.5% after 4 h and revealed excellent stability under visible light. The superoxide radicals, holes and hydroxyl radicals played a crucial role, which causing the damage of cell wall and membrane, the bleaching of pigments, the collapse of superoxide dismutase and hydrogen peroxidase and other oxidation stress effects. Above all, Ag/AgCl@ZIF-8 sponge fabricated from this simple and cost-effective dip-coating method has a promising prospect for the removal of harmful cyanobacteria in eutrophic water bodies.

1. Introduction

Cyanobacterial harmful algal blooms (CyanoHABs) are a great threat to the aquatic ecosystem and drinking water reservoirs worldwide, which has become more severe and frequent due to eutrophication and climate-change effects [1]. *Microcystis aeruginosa* (*M. aeruginosa*) is one of the most harmful cyanobacteria which would produce cyanotoxins that lead to digestive and skin diseases, neurological impairment and even death [2]. Therefore, it is imperative to prevent, control and mitigate the global expansion of CyanoHABs.

Strategies aimed at controlling and mitigating harmful blooms have focused on physical [3],chemical [4], and biological [5] approaches. Many of these strategies show promise but are currently difficult to achieve safe and efficient application in large areas of natural water bodies. Fan et al. [6] pointed out that ultrasound inhibited the physiological, metabolic activity of *M. aeruginosa*, and the proportion of damaged algae cells was proportional to ultrasonic power density. However, it is infeasible in applying ultrasonic radiation on a large scale in the real water bodies. Kondzior et al. [7] proposed that the chlorophyll *a* content of algae was reduced by 63% when treated with $CuSO_4$ algaecide (0.15 mg/L) for 7 d, while $CuSO_4$ algaecide has a disadvantage of environmental persistence and biological toxicity in the application. Maarten et al. [8] found that *Egeria densa* and *Potamogeton illinoensis* can be used to control phytoplankton biomass. However, biological control takes a long period of time to work in water bodies. Therefore, photocatalysis has been favored in recent years due to its proven potential in contaminant removal (e.g., easy to obtain, low cost, clean-up of a wide range of pollutants and no secondary pollution) [9].

Photocatalysis is a light-driven chemical reaction that requires photocatalysts, which are basically semiconductors. Reactive oxygen species (ROSs), which are produced by photocatalysts, cannot only react with the cell surface, and then damage the cell wall and membrane permeability, but also degrade a variation of metabolites (e.g., algal toxins and odorous substances) [10,11]. TiO_2, the first semiconductor material found for photocatalysis, normally can be activated by ultraviolet light (320 nm < λ < 400 nm). However, its application as a catalyst for algae bloom control is limited due to its wide band gap (E_g = 3.2 eV) [12]. Hence, there is an essential task for us to explore and modify a novel photocatalyst to achieve the narrower band gap and the broader response range of the visible light (λ > 400 nm).

* Corresponding author at: College of Civil Engineering, Fuzhou University, 350116 Fujian, China.
E-mail addresses: fgdfz@fzu.edu.cn, cqufgd@126.com (G. Fan).

https://doi.org/10.1016/j.apcatb.2019.117866
Received 18 April 2019; Received in revised form 7 June 2019; Accepted 13 June 2019
Available online 19 June 2019
0926-3373/ © 2019 Elsevier B.V. All rights reserved.

Metal-organic frameworks (MOFs) are a new class of porous crystal nanomaterials with periodic multidimensional network structures, which are formed by the self-assembly of organic ligands such as metal ions and aromatic polyacids through coordination [13]. To date, many efforts have been directed to photocatalytic inhibition of algae growth by nanomaterials. Sathe et al. [14] found that *Dunaliella salinifera* was adsorbed on the surface of ZnO nanorods under visible light and then inactivated by free radicals. Wang et al. [15] found that inactivation of *E. coli* K-12 by using g-C_3N_4/red P composites (CNP) as a photocatalyst caused the level of CAT significantly increased under O_2 aeration condition and slightly increased under N_2 aeration condition, while no CAT activity was induced under dark conditions. Wang et al. [16] reported that about 90% of chlorophyll *a* in algae cells was degraded after 3 h of photocatalytic reaction under a tungsten halogen lamp using algae-TiO_2/Ag hybrid nanomaterial. The authors inferred that the photocatalysis of nanomaterials mainly inhibits the growth of algae cells by adsorption and ROSs oxidation which destroy the antioxidant enzyme system. However, the mechanisms of photocatalytic nanomaterials acting on the physiological characteristics of algae cells are still under study.

As the most popular substance for enhancing bactericidal activity, silver species (Ag) has great potential in constructing composite photocatalysts for microoganism inactivation because of the surface plasmon resonance (SPR) effect and electron trapping ability of Ag nanoparticles [17]. Many Ag-containing nanostructured photocatalysts have been made to enhance light absorption including Ag/g-C_3N_4 [18], Ag/TiO_2 [19] and Ag/ZnO [20]. In particular, Silver halides decorated with silver (Ag/AgX), a class of highly efficient visible-light-driven photocatalyst, exhibit high absorption in the visible region as well as photogenerated electron-hole pair separation [21]. However, aggregation of the Ag/AgX particles, the short lifetime of the photogenerated electron–hole pair, and the limited visible-light response has resulted in unsatisfactory photocatalytic efficiencies [22]. Among the many kinds of MOFs, zeolitic imidazolate framework 8 (ZIF-8) has attracted wide attention in catalysis due to their commercial availability, large surface area and outstanding performance on thermal and chemical stability. The combination of Ag/AgCl with ZIF-8 forms p-n heterojunctions which greatly enhance the efficiency of photoinduced charge separation under visible light irradiation. According to our previous study [23], the photogenerated electrons can reduce oxygen molecules adsorbed on the surface of Ag/AgCl@ZIF-8 to $O_2^{\cdot -}$, thus further improves the photocatalytic performance of catalyst.

The difficulty of the separation and recycling of nano-size materials is one technology challenge in the application of photocatalyst in ecosystems, is mainly due to the secondary pollution caused by the powdery photocatalyst [24]. Meanwhile, CyanoHABs dominantly breaks out on the surface layer of water bodies, and thus the traditional homogeneous system results in unsatisfactory photocatalytic efficiencies. To solve these problems, floating photocatalysts have recently attracted tremendous attention in algae inhibition [25]. It has been reported that MOFs are more adjustable in function and structure than TiO_2 with the larger specific surface area [26,27]. Based on these advantages, MOFs are often used to be coated on other substrates to assemble a floating photocatalyst. The floating MOF catalysts can avoid the large number of nano-materials dispersed into the natural water bodies and simultaneously be well contacted with the surface harmful cyanobacteria to achieve great photocatalytic efficiencies. Besides, no survey was conducted on the control of CyanoHABs using this novel Ag/AgCl@ZIF-8 coated sponge. Therefore, we expected the MOF coating suitable for the water remediation in algae inactivation and contaminant removal.

In this paper, a new MOF-based floating photocatalyst (Ag/AgCl@ZIF-8 coated sponge) was synthesized via a simple dip-coating method and characterized by X-ray diffraction (XRD) and field emission scanning electron microscopy (FESEM). The impacts of MOF coating on *M. aeruginosa* were also investigated including the morphology, intracellular organic matters (IOM), extracellular organic matters (EOM), photosynthetic system, antioxidant enzyme system, and other physiological characteristics. Finally, a possible mechanism was proposed to elucidate the photocatalytic inactivation process induced by Ag/AgCl@ZIF-8 coating under visible light.

2. Materials and methods

2.1. Preparation of Ag/AgCl@ZIF-8 coating and characterization

The Ag/AgCl@ZIF-8 was synthesized with minor modification according to Gao et al. [22]. Briefly, 0.2 g of ZIF-8 was dissolved in 14 mL of 53.7 mM $AgNO_3$ water : ethanol (v/v = 1 : 6) mixture under 3 h of magnetic stirring. Subsequently, the obtained solution was added dropwise into 23 mL of 40 mM NaCl water : ethanol (v/v = 1 : 6) solution within 20 min. After being stirred at room temperature for 10 h, the color of resultant solution changed from white to light blue. The products was obtained by centrifugation, washed with deionized water for three times, and dried in an oven at 70 °C for 12 h.

The polyurethane sponge was cut into blocks (4.5 cm × 4.5 cm × 0.5 cm) and washed by ultrapure water to remove particle contaminants. Then, the blocks were ultrasonically cleaned several times in ultra-pure water and ethanol and dried at the oven. Two treated sponges were immersed into 50 mL of 3.0 g/L sodium dodecyl benzene sulfonate (SDS) solution followed by shaking on a thermostat shaker for 30 min. After that, the sponges were taken out, soaked in ultra-pure water to remove the excess SDS, and dried in the oven to give SDS modified sponges. In order to obtain a coated sponge, a dip-coating method was introduced. Typically, a certain amount of Ag/AgCl@ZIF-8 was dissolved in ultrapure water followed by ultrasonication for 15 min to obtain an Ag/AgCl@ZIF-8 aqueous solution of 2.5 g/L. Two modified sponges were then taken out and immersed into 50 mL of the solution and shaken on a thermostat shaker for 2 h. In order to prevent catalyst precipitation, the modified sponges were flipped every few minutes to evaporate the surface moisture at 363.15 K in the oven. The Ag/AgCl@ZIF-8 coated sponge was obtained by drying for 12 h. To probe into the difference between SDS-modified sponge and non-modified sponge, Ag/AgCl@ZIF-8 was loaded on a blank sponge as the control group.

XRD was recorded by an Ultima IV high-resolution X-ray diffraction system (Rigaku, Ultima IV, Japan) with Cu Kα radiation (λ = 0.15418 nm) at a scanning speed of 20°/min, in the 2θ range from 5° to 75°. The morphologies and structure of prepared materials were observed using a FESEM (Hitachi, S-4800, Japan).

2.2. Photocatalytic experiment

2.2.1. Algae cultivation

M. aeruginosa (FACHB-905) was provided by the Freshwater Algae Culture Collection at the Institute of Hydrobiology (FACHB). The algae were cultivated using BG-11 medium in an incubator at 298.15 K with an illumination of 2000 lx provided for 14 h every day at 30 ± 1 in BG-11 (Blue-Green Medium) [28]. The conical flask was shaken three times a day to prevent deposition of the cells. *M. aeruginosa* was cultured until the density approximately reached 6.48 × 10^6 cell/L (corresponding to OD_{680} ≈ 0.43) which was close to the density when harmful cyanobacteria blooms occurred in natural water bodies.

2.2.2. M. aeruginosa removal efficiency

Inhibition on algae growth was indicated by chlorophyll *a* [29]. The content of chlorophyll *a* was measured referred to China EPA standard methods [30]. Based on the changes of chlorophyll *a* concentration, which was proportional to algal cell numbers in the samples, the percentage of cells removed by Ag/AgCl@ZIF-8 coating was simplified as the “removal efficiency”. The removal efficiency of *M. aeruginosa* can be calculated by the following formula:

$$\text{Removal efficiency (\%)} = (1 - C_t/C_0) \times 100 \quad (1)$$

Where C_0 and C_t represent the initial chlorophyll *a* content (mg/L) at the initial time and *t*-hour, respectively.

2.2.3. Photocatalytic inhibition of M. aeruginosa

Experiments were carried out in a home-made photochemical reactor following the same procedures described in our previous study [31]. The photocatalytic experiments were conducted for 6 h and samples were collected at pre-determined intervals. The coated sponge was washed with ultrapure water to remove the excess Ag/AgCl@ZIF-8 attached to the surface before using. 100 mL of cultured algae suspension and a piece of MOF coated sponge were added into a 250 mL sandwich beaker. 8 mL of algal cell suspension for each sample was taken out to determine the chlorophyll *a* content. After the photocatalytic experiments, the MOF coated sponge was taken out, washed thoroughly with ultrapure water, and dried at 343.15 K. The stability of photocatalyst was obtained by the repeated use of the photocatalyst coating for four runs under identical conditions. The control group was conducted using a sponge with no photocatalyst.

2.3. Analytical methods

2.3.1. Cell membrane integrity assay

At pre-determined time intervals of 1 h,5 mL of suspension was withdrawn and centrifuged (4500 r/min, 10 min). 1 mL of 1 mg/L Propidium Iodide (PI) was added into the precipitates, and the suspension was dark-adapted at room temperature for 30 min. After this, the integrity of algae cell s was examined by the flow cytometry (FACSCalibur, Beckman Coulter, USA) at 488 nm with data analyzed using Cell-Quest software. PI fluorescence was collected by the FL3 channel, and the number of cells collected by FL3 was 10,000.

2.3.2. Cell membrane permeability assay

At pre-determined time intervals of 1 h, 5 mL suspension was withdrawn, centrifuged at 4500 r/min at 4 °C for 10 min. The exudation of intracellular organic matter (IOM) was indicated by the absorbance of the supernatant at 264 nm.

2.3.3. Extraction and determination of total soluble protein

The extraction of total soluble protein was referred to Tao et al. [32]. At pre-determined time intervals of 1 h, 5 mL of suspension was centrifuged at 4500 r/min at 4 °C for 15 min to collect the precipitates. The precipitates were homogenized with 1 mL of phosphate buffer solution (PBS). The resultant mixture was centrifuged, and the supernatant was discarded. This procedure was repeated twice. Cell extracts were prepared by addition of a 100 μL protein lysis buffer[containing 250 mM Tris base, 2% SDS, 0.5 mM EDTA and 10% glycerol] followed by subsequent ultrasonic(4 × 30 s, 200 W, 5 s interval) on an ice bath. The supernatants were harvested by centrifugation at 5000 r/min at 277.15 K for 20 min and stored at 193.15 K for further analyzing.

The protein concentration was determined by the bicinchoninic acid (BCA) protein assay kit according to the method of Wei et al. [33]. First, Cu^{2+} is reduced to Cu^{+} under alkaline conditions. Then Cu^{+} continues to react with the BCA reagent to form a purple complex. Subsequently, the absorbance value (OD_{562}) at the wavelength of 562 nm is measured by the enzyme-labeling instrument (ELX800, Bio Texk, USA) to obtain the relationship curve between the protein concentration and OD_{562}. Finally, the protein concentration could be obtained through calculation.

2.3.4. Extraction and determination of phycobiliproteins

The phycobiliproteins of *M. aeruginosa* mainly consist of phycocyanin (PC), phycoerythrin (PE) and allophycocyanin (APC) [34]. The extraction of phycobiliproteins was referred to the procedure of Padgett et al. [35]. First, 8 mL samples were centrifuged to collect the precipitates, and the precipitates were washed with 1 mL of PBS and centrifuged again. This process was repeated three times. Then, the mixture was homogenized with 4 mL PBS, frozen at -20 °C for 1 h and thawed at room temperature in darkness. This procedure was repeated three times. Finally, the supernatants were harvested by centrifugation for 10 min at 4500 r/min. The absorbance at the wavelength of 565 nm, 620 nm and 650 nm were measured, which were marked as OD_{565}, OD_{620} and OD_{650} respectively. The content of PC, APC and PE and the relevant content of PBP were calculated according to the following formulas [32]:

$$PC\,(mg/L) = \frac{OD_{620} - 0.7 \times OD_{650}}{7.38} \quad (2)$$

$$APC\,(mg/L) = \frac{OD_{650} - 0.19 \times OD_{620}}{5.65} \quad (3)$$

$$PE\,(mg/L) = \frac{OD_{565} - 2.8 \times PC - 1.34 \times APC}{1.27} \quad (4)$$

$$\text{PBPs} = \text{PC} + \text{APC} + \text{PE} \quad (5)$$

$$\textit{Relevant content of PBP} = \frac{\text{content of the experimental group}}{\text{content of the control group}} \quad (6)$$

2.3.5. Extraction and determination of antioxidant enzymes

The effect of MOFs on algal antioxidant enzymes system includes superoxide dismutase (SOD) and hydrogen peroxidase (CAT). The activity of SOD/CAT was determined by Kits from Nanjing Jiancheng Bioengineering Institute. For each sample, algae cells were harvested by centrifugation at 4500 r/min for 10 min and diluted in 1 mL PBS. After that, the suspension was ultrasound-treated by an ultrasonic cell disrupter (VCX130, Sonics & Materials Inc, USA). Subsequently, the supernatant was collected by centrifugation for the analysis of enzyme activity.

2.3.6. Extraction and determination of organic matter

According to Qu et al. [36], high-speed freeze centrifugation was applied to extract extracellular organic matter (EOM) from algae cells, and an ultrasonic cell disrupter was employed to release intracellular organic matter. A fluorescence spectrum scanning (FS5, Edinburgh, UK) was applied for the determination of algal organic matters with the data processing using MATLAB software (Mathworks, Inc, Natick, MA) [37]. The scanning range of the *M. aeruginosa* cell suspension ranged from excitation wavelength Ex: 200–750 nm, emission wavelength Em: 200–800 nm, and slit width 5 nm. The EOM scanning range of algae cells ranged from excitation wavelength Ex: 200–450 nm, emission wavelength Em: 200–550 nm, and slit width 6 nm. The IOM scanning range of algae cells ranged from excitation wavelength Ex: 200–450 nm, emission wavelength Em: 200–550 nm, and slit width 9 nm. The step size was set uniformly to 5 nm, and the detection cell was a 1 cm quartz fluorescence sample cell. Meanwhile, the three-dimensional fluorescence spectra of ultrapure water were tested as blank correction results.

2.3.7. Zeta potential determination

Zeta potentials for the algal cells were measured by using a laser particle size analyzer (Zetasizer Nano ZS, Malvern, UK). At pre-determined time intervals of 1 h, five mL of the control and experimental groups were withdrawn simultaneously, and the testing temperature was set at 248.15 K.

2.4. Quenching experiment

2.4.1. Reactive radicals

Reactive oxygen species quenching experiments were conducted to reveal the mechanism of the photocatalytic process. Isopropanol (IPA,

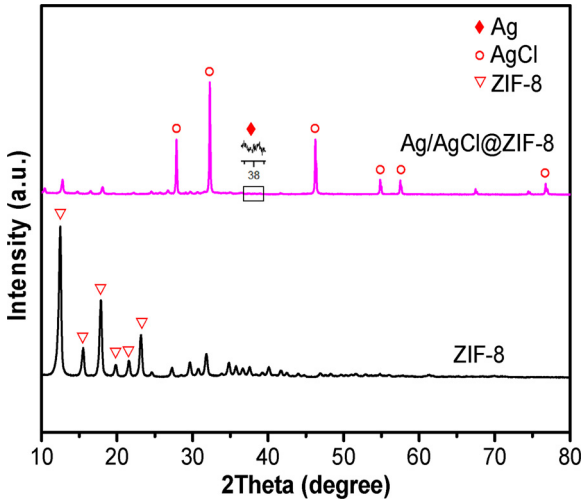

Fig. 1. XRD patterns of ZIF-8 and Ag/AgCl@ZIF-8.

1 mM), benzoquinone (BQ, 1 mM) and sodium oxalate (SO, 1 mM) were added respectively into the algal solution treated by Ag/AgCl@ZIF-8 coated sponge to trap hydroxyl radicals (·OH), superoxide radicals ($O_2^{\cdot -}$), and holes (h^+). The experimental process was same to the photodegradation experiments except for the addition of scavengers.

2.4.2. FTIR analysis

The algae cells were treated according to 2.2.3. An 8 mL volume of each sample was harvested by centrifugation and washed with PBS for three times before freeze-dried. The dried algal cells were mixed with KBr powder, fully ground and then tableted with a rotary press. Fourier Transform Infrared Spectra (FTIR) were recorded on a Nicolet (iS50, Thermo Scientific, USA) from 400 to 4000cm^{-1}.

3. Results and discussion

3.1. Characterization of as-prepared nanoparticles and MOF coating

The XRD patterns of ZIF-8 and Ag/AgCl@ZIF-8 are presented in Fig. 1. The sample of ZIF-8 showed distinct peaks at 7.39°, 10.42°, 12.79°, 14.73°, 16.49° and 18.07°, which were ascribed to the (011), (002), (112), (022), (013), and (222) reflections of ZIF-8, respectively [38]. New peaks presented at 27.8°, 32.2°, 46.2°, 54.8°, 57.5° and 76.7° were ascribed to the (111), (200), (220), (311), (222), and (420) reflections of AgCl, respectively [39]. The peak at 38.2° was due to the cubic phase of Ag (111). All peaks were sharp and clear, and no other characteristic peaks were found, indicating that the synthesized Ag/AgCl@ZIF-8 had good crystal morphology and possessed high purity.

Fig. 2 presents the morphology of all samples observed by using a FESEM. The SEM image of ZIF-8 reveals that ZIF-8 had a smooth surface with grain diameter ranging from 0.5 to 1.5 μm (Fig. 2a). As shown in Fig. 2b, there were many disc-like structures stacked together on the surface of AgCl. Ag/AgCl@ZIF-8 was covered with small particles of nanometer scale to form a rough surface, which was mainly because the composite of ZIF-8 increased the surface area of Ag/AgCl (Fig. 2c). These nanoparticles could also increase active sites for pollutant degradation. Moreover, there was no obvious aggregation observed on the sponge surface and the sponge skeleton was mainly covered by the layer of Ag/AgCl@ZIF-8, suggesting that the Ag/AgCl@ZIF-8 nanocrystals were well-distributed on the sponge surface (Fig. 2d). All the above indicate that MOFs can be uniformly and efficiently loaded on floating carriers.

It was obvious from the Fig. S1 that the SDS-modified sponge had more Ag/AgCl@ZIF-8 nanocrystals attached on the sponge surface, suggesting that the modification of SDS facilitated the adsorption performance of the carrier. According to our previous study [23], the zeta potential of Ag/AgCl@ZIF-8 exhibited a positive surface charge in neutral environment. However, SDS was found to be negatively surface-charged and even the sponge itself could exhibit a slightly negative-charge on its surface [40]. It has been suggested that MOFs can interact with organic pollutants through specific interactions (e.g., acid–base interaction, π-complex formation, π–π interaction, H-bonding) [41]. The positive charge of Ag/AgCl@ZIF-8 could be attracted to SDS through the electrostatic effect. Additionally, it has been suggested that 2-methylimidazole of ZIF-8 contained an imidazole ring, which could be considered as an aromatic compound and might be also attracted to the SDS surface through the π-π interaction with a benzene ring of SDS. Thus, Ag/AgCl@ZIF-8 was adsorbed onto the sponge primarily via the electrostatic effect and possibly by the π-π interaction. Without the addition of SDS offering more accessible adsorption sites, Ag/AgCl@ZIF-8 nanocrystals detached from the blank sponge and dissolved in the aqueous solution after oscillation. Therefore, the addition of SDS resulted in noticeable effects on the Ag/AgCl@ZIF-8-loading to sponge.

3.2. Photocatalytic inactivation of M. aeruginosa

As shown in Fig. 3, the concentration of chlorophyll *a* was found to decrease by only 10% and 15% with ZIF-8 and Ag/AgCl, respectively. This indicates that ZIF-8 and Ag/AgCl had low photocatalytic activity to inhibition on the growth of *M. aeruginosa* under visible light. In comparison, the composite Ag/AgCl@ZIF-8 exhibited higher photocatalytic performance under visible light, and the MOF coating prepared by dip-coating maintained the highest photocatalytic activity under visible light. When the photocatalytic reaction was carried out for 1 h by Ag/AgCl@ZIF-8 coating, the removal rate of chlorophyll *a* reached 20% which demonstrated the nearly same inactivation efficiency following 2 h of Ag/AgCl@ZIF-8 powder. The removal rate of chlorophyll *a* was as high as 98% after 4 h, and 99.9% of chlorophyll *a* was degraded at the end of the experiments. The Ag/AgCl@ZIF-8 coated sponge could adsorb a large amount of algal cells, which may due to i) the hydrophilicity of sponge could be greatly improved because of the layer of ZIF-8 and the assistance of SDS [40], and ii) the physical adsorption as polyurethane sponge itself is porous material. Then, a part of damaged *M. aeruginosa* desorbed from sponge and returned into solution after interacting with Ag/AgCl@ZIF-8 loaded on the sponge surface.

The change of the removal rate of chlorophyll *a* in four recycling runs of photocatalytic degradation experiments is presented in Fig. 4. The coated sponge displayed stable photocatalytic performance, which still removed 94% chlorophyll *a* after four cycles of photocatalytic experiments. The decrease of catalyst activity may due to the loss in recovery washing. The reason why the coated sponge was better than the powder in photocatalytic inactivation and removal of algae was that the sponge floats on the surface of water and can directly utilize the photon energy, while in the homogeneous system the visible light is absorbed and reflected by the algae liquid when irradiated onto the surface of the catalyst. Therefore, the floating catalyst can improve the utilization of photons. Besides, there are no obvious Ag/AgCl@ZIF-8 solids observed at the bottom of the beaker after four cycles, and no significant change can be found on the surface of the carrier, which reveals that the modified sponge prepared by dip-coating exhibit a great adhesion capability.

3.3. Effects on physiological characteristics of M. aeruginosa

3.3.1. Integrity of cell membrane

The changes in cell membrane integrity in the photocatalytic inactivation of algae by Ag/AgCl@ZIF-8 coating is shown in Fig. 5. The M1 and M2 regions showed in flow cytometry results indicated the intact and damaged membrane, respectively. The fluorescence intensity of M1 region was proportional to the number of living cells while M2 region indicated the damaged algal cells. In the control, the

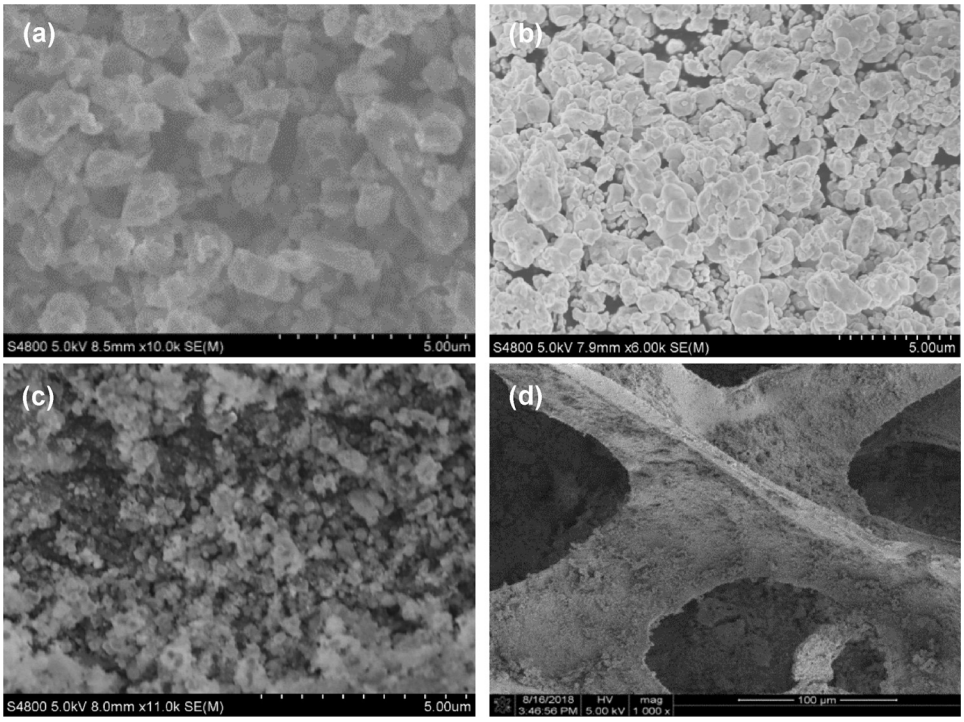

Fig. 2. SEM images of (a) ZIF-8, (b) Ag/AgCl, (c)Ag/AgCl@ZIF-8 and (d) sponge with Ag/AgCl@ZIF-8.

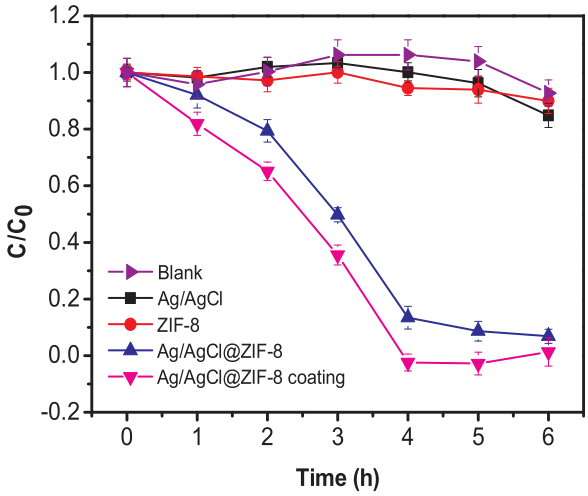

Fig. 3. Comparison of the removal efficiency without of photocatalyst, and the use of Ag/AgCl, ZIF-8, Ag/AgCl@ZIF-8 and Ag/AgCl@ZIF-8 coating. (C_0 = 2.74 mg/L, catalyst = 10 mg/L, pH = 7.0).

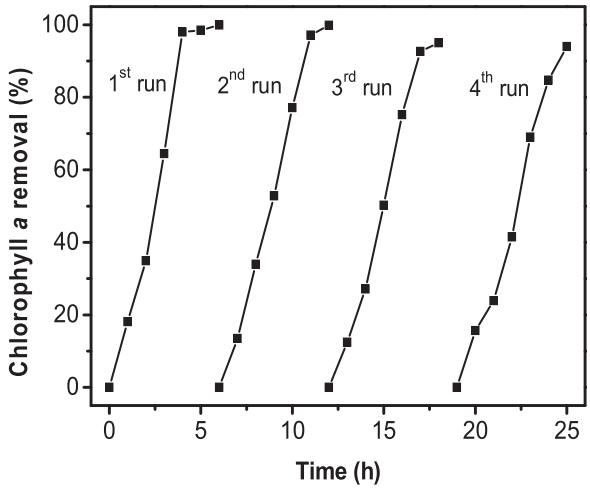

Fig. 4. Changes in the chlorophyll *a* removal for the photocatalytic inactivation of *M. aeruginosa* in four successive cycles.

fluorescence intensities of the M1 region maintained high and were always greater than that of the M2 region, showing that most of *M. aeruginosa* were living cells at the beginning of experiment. The sponge with no photocatalyst had little effects on the growth of *M. aeruginosa* under visible light, and the cell membrane maintained a high integrity. In comparison, the fluorescence intensities of the experimental group were basically in the M2 region after 1 h of exposure. This indicated that *M. aeruginosa* of the experimental group suffered significant cell damage. With the photocatalytic process extended to 5 h, there was almost no fluorescence peak detected in the M1 region, implying that the Ag/AgCl@ZIF-8 coating is efficient in damaging the cell membrane.

As samples contained both intact and damaged algal cells, the counting and quantitation of cells were carried out using Cell-Quest software. In the control, a small group of the algae (i.e., about 13% of the total counts) were assigned to damaged membrane in the beginning of experiments. These apoptotic cells were the result of cell metabolism in the incubation. The proportion of intact cells in the control group decreased from 87% to 79% after 1 h of irradiation, and there was no significant decrease subsequently (Fig. 6). However, the damaged cells proportion of the experimental group reached 98% when the photocatalysis conducted for 1 h. When the photocatalysis extended to 3 h, there were barely living cells with an intact membrane observe. These results indicate that the Ag/AgCl@ZIF-8 coating caused irreversible damage to *M. aeruginosa* during photocatalysis, and the sponge was not responsible for the mass death of algal cells.

3.3.2. Permeability of cell membrane

Since cell membrane damage would lead to the leakage of electrolyte and non-electrolyte. The optical density (OD) of UV-absorbing at 264 nm was reported to determine the non-electrolyte components in extracellular exudate, which can serve as an indicator of mild or strictly

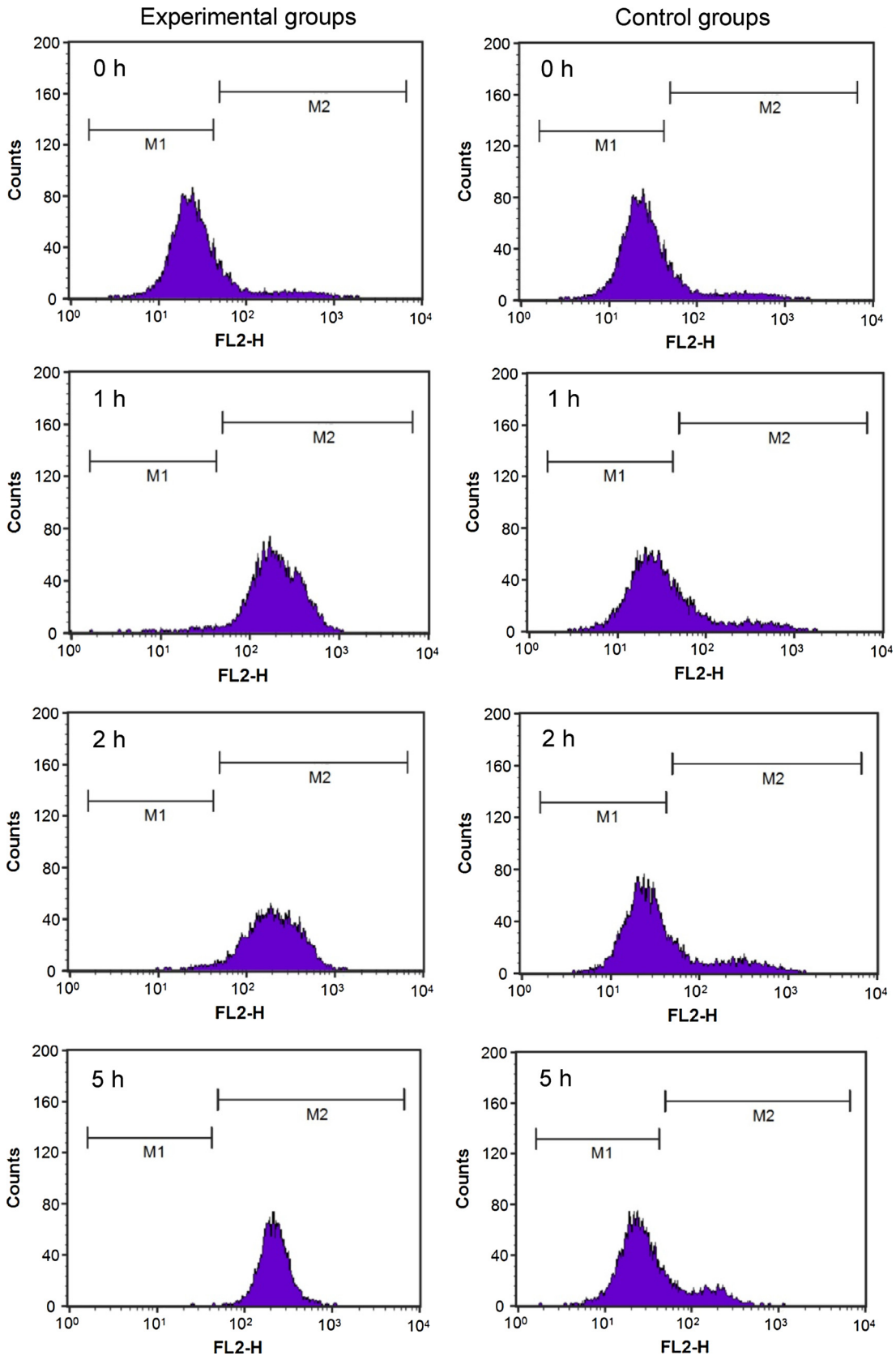

Fig. 5. Flow cytometry analysis with Propidium Iodide (PI) staining following photocatalytic inactivation of *M. aeruginosa* by Ag/AgCl@ZIF-8 coating. M1: intact membrane; M2: damaged membrane. Axes: FL2-H corresponds to PI fluorescence detected at 488 nm.

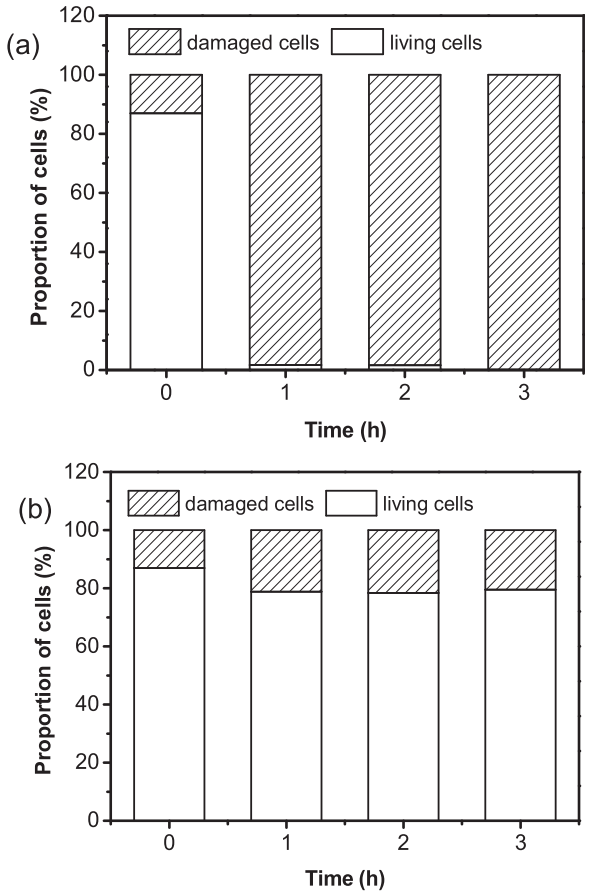

Fig. 6. The ratio of damaged cells to living cells in the photocatalytic inactivation of *M. aeruginosa* with the use of Ag/AgCl@ZIF-8 coating (a) experimental groups and (b) control groups.

localised degrees of cell membrane damage [42].

The experimental group released a certain amount of extracellular exudate after 1 h of irradiation (Fig. 7), which implies that the permeability of the cell membrane increased and the cell membrane had been damaged. The permeability of *M. aeruginosa* membrane increased consistently over time and reached its maximum at 6 h. This indicates that the permeability increased as soon as the photocatalysis started and several extracellular exudates are released. In contrast, there was no significant change in the permeability of the control group in the first 4 h. This may due to most of the algal cells membrane were not damaged in the control group according to the results of flow cytometry (Fig.5).The OD_{264} started to increase under irradiation for 5 h but was still lower than that of the experimental group at 1 h.

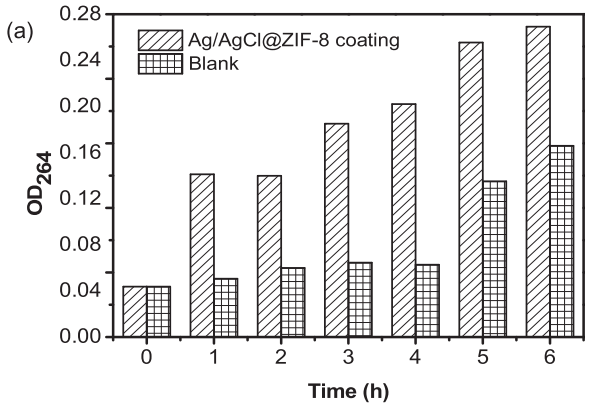

Fig. 7. The OD_{264} values of *M. aeruginosa* between different groups.

3.3.3. Total soluble protein

Protein is not only an essential part of the organism but also acts as an enzyme to promote biochemical reaction in cell metabolism. Therefore, the content of soluble protein can reflect the activity of cell metabolism to a certain extent [43]. The protein standard curve based on the protein concentration and OD_{562} showed good linearity with the coefficient of determination (R^2) of 0.9966 (Fig. 8a) and was used for the quantitative detection of algal cell protein. The total soluble protein content in the control group was initially 26.45 mg/L, and fluctuated in a small range with the content of 22.59 mg/L at the end of the experiment (Fig. 8b), which attributed no significant decrease during the photocatalysis treatment, indicating that the growth of algal cells in the control group was not inhibited. However, the total soluble protein content of the experimental group decreased to 22.12 mg/L after 1 h, which was 16.4% lower than the initial content. After 3 h of irradiation, the total protein content of the algal cells decreased to 13.98 mg/L, which was lower than that of the initial and the control group by 47.15% and 46.1%, respectively. At the end of the reaction, the total protein content of the algal cells dropped to 4.04 mg/L, which was 15.3% of the initial level. According to these results, we infer that the reason why the total protein decreased in the first hour was mainly that the cell membrane was damaged and then ROS oxidized organelles would inhibit the protein synthesis. As the cell membrane was further destroyed, intracellular materials leaked and a large number of proteins were lost, eventually leading to the death of cells.

3.3.4. Phycobiliprotein (PBP)

Phycobilin (PB) is the main photosynthetic pigment in cyanobacteria, which is often combined with proteins to form phycobiliproteins (PBPs) [44]. The PBPs of *M. aeruginosa* can be divided into three types: PC, APC, and PE, which is attached to the external surface of thylakoid lamella [45]. Fig. 8c-f shows the relevant content of PB and PBPs during the photocatalysis treatment.

The relevant content of PC drops rapidly within 1 h, which is about 9% of the control group and remains the same subsequently (Fig. 8c). The relative contents of APC, PE, and PB all decreased significantly in the first 2 h and then stabilized, which exhibited the same trend (Fig. 8d-f). The reason why the relative content increases in the experimental group at 6 h can be attributed to the decrease of PBPs and PB content in the control group. Wang et al. [46] found that H_2O_2 entering cells could lead to the separation of PBPs from the thylakoid membrane. Thus, we speculate that the Ag/AgCl@ZIF-8 coating would generate ROS under visible light, which can cause damage to PBPs and water-soluble pigments (PB), affecting the normal function of the photosynthetic system, thereby inhibiting the growth of algae cells. Besides, the destruction of the water-soluble pigments reconfirms that the MOF coating can efficiently remove algae under visible light.

3.3.5. Antioxidant enzyme system

SOD and CAT are two important antioxidant enzymes in algae cells, which can respond to environmental stress. Enzymes with SOD can dismutate $O_2^{\cdot -}$ into hydrogen peroxide [47]. CAT defends against oxidative stress from the environment and a higher CAT activity indicates that algal cells are encountering a more significant H_2O_2 attack [48].

As shown in Fig. 9a, SOD activity of the control group was initially about 4.5 U/mL, and increased in the first 3 h following by a decrease to the initial level. Algal cells were adapted to the environmental stress after 6 h of treatment and SOD activity decreased to the initial level. This suggests that the sponge with no photocatalyst could not damage the SOD of algal cells under visible light. Conversely, the SOD activity of the experimental group sharply increased within 1 h, which was 3 times higher than the initial level, and reduced slightly with remaining at a relatively high level. SOD activity in all treatment groups was

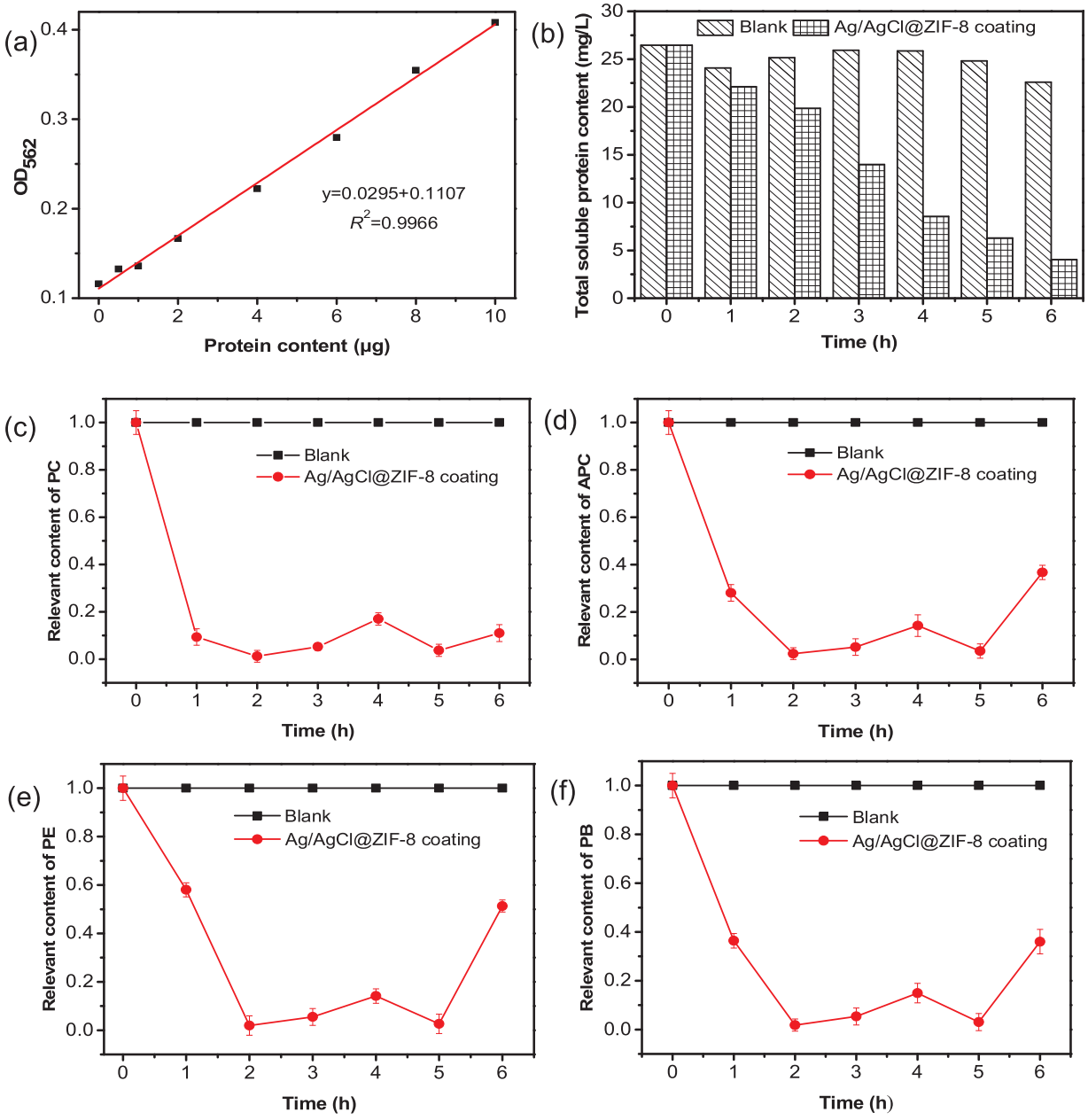

Fig. 8. (a) Standard linear curve between protein and OD_{562}; (b) Changes in total soluble protein content and the changes of content in (c) phycocyanin, (d) allophycocyanin, (e) phycoerythrin, and (f) phycobiliprotein during photocatalytic inactivation of *M. aeruginosa* by Ag/AgCl@ZIF-8 coating.

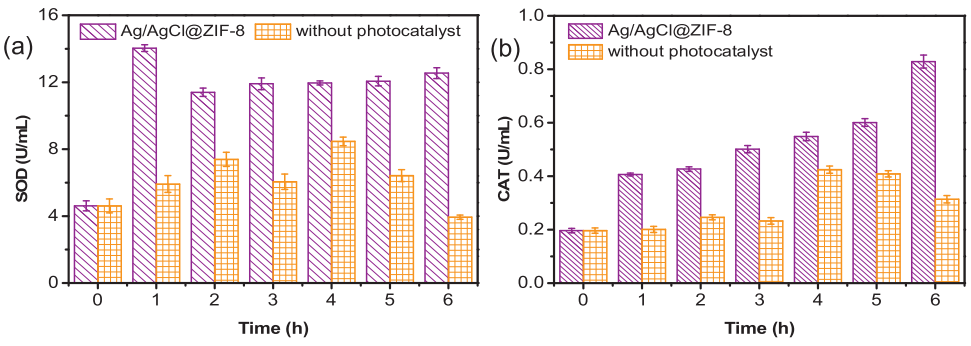

Fig. 9. Changes of (a) SOD and (b) CAT activities during photocatalytic inactivation of *M. aeruginosa* by Ag/AgCl@ZIF-8 coating.

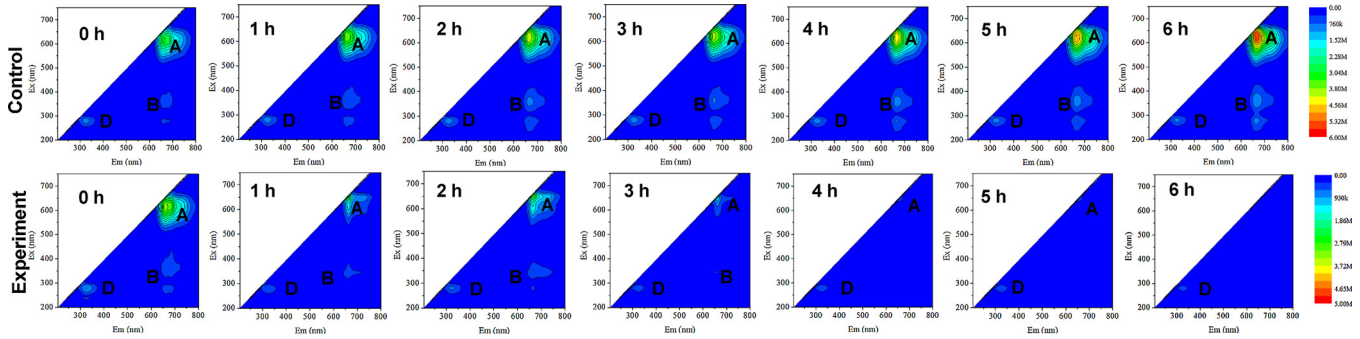

Fig. 10. Three-dimensional fluorescence spectrum of algae cell suspension during photocatalytic inactivation of *M. aeruginosa* by Ag/AgCl@ZIF-8 coating.

higher than in the control group. The increase in SOD activity was mainly because algal cells were stimulated by light irradiation to extensively activate SOD to defend oxidative damage induced by MOF coating. This result implies that as soon as ROS is produced by catalyst under visible light, the algal cells would suffer continuous damage.

As shown in Fig. 9b, the CAT activity of the control group did not significantly change in the first 4 h but slightly increased at 5 h, then reduced at the end of the experiment. No significant change of CAT activity in the early stage of treatment was observed since CAT was sufficient enough to remove H_2O_2 from algae cells. However, H_2O_2 was accumulated in cells in the later stage, thus increasing CAT activity until excess H_2O_2 was removed. On the other hand, the CAT activity of the treated group gradually increases over time and reaches the maximum value at 6 h. This indicates that H_2O_2 is produced and accumulated as soon as the photocatalytic degradation begins, and finally exceeds the limit value of CAT, leading the collapse of the antioxidant enzyme system.

3.3.6. IOM and EOM

The fluorescence spectra of different portions of algae suspension are presented in Fig. 10. It was observed that the fluorescence spectrum of algae solution contained peak A, $\lambda_{ex}/\lambda_{em}$ = 620/650 nm; peak B, $\lambda_{ex}/\lambda_{em}$ = 440/680 nm; peak D, $\lambda_{ex}/\lambda_{em}$ = 275/340 nm, which represent PC, chlorophyll *a*, tryptophan and tyrosine, respectively [49–51]. The fluorescence spectrum of the control group increased over time, suggesting that algal cells were not inhibited during the photocatalytic treatment. A reduction in the intensities of peaks A, B, and D in the treated group indicates that algal cells were inactivated by Ag/AgCl@ZIF-8 coating. This is well consistent with the results obtained in section 3.2. With the treatment time extended to 6 h, the intensities of peaks A, B, and D disappeared, suggesting that the removal of *M. aeruginosa* under visible light is a continuously efficient process.

Three peaks were observed in the fluorescence spectrum with $\lambda_{ex}/\lambda_{em}$ = 280/325 (peak A), 255/455 (peak C), and 345/425 (peak D) (Fig. S6), which were reported to be indicators of protein-like, fulvic acid-like and humic-like substances, respectively [52]. The intensities of peaks A, C, and D grew strong over time, indicating that the sponge with no photocatalyst does not inhibit the growth of algal cells. However, in the experimental group, the intensity of peak A gradually reduced whereas peaks C and D strengthened. This suggests that most fulvic acid-like and humic-like substances are converted by protein-like substance and released by algal cells under photocatalytic treatment using Ag/AgCl@ZIF-8 coating.

The IOM fluorescence spectrum of the initial algal solution contains four fluorescence peaks, which are denoted as peak A ($\lambda_{ex}/\lambda_{em}$ = 275/320), peak B ($\lambda_{ex}/\lambda_{em}$ = 225/325), peak C ($\lambda_{ex}/\lambda_{em}$ = 275/450), and peak D ($\lambda_{ex}/\lambda_{em}$ = 350/450), respectively (Fig. S7). Peak A represents microbial soluble metabolites, aromatic proteins, and phenolic substances; peak B indicates aromatic substances such as tyrosine, tryptophan, fulvic acid-like and humic acid-like substances corresponded to peaks C and D [53]. There is no significant increase in peak intensities observed in the control group, suggesting that the sponge with no photocatalyst does not inhibit algal cells under visible light. Conversely, the fluorescence peaks intensities of IOM in the algal cells of the experimental group decreased continuously. Notably, the decrease in peak A and peak B suggests that MOF coating cause mass death of algal cells under visible light since peaks A and B are indicators of the biochemical organism which reflect the cell activity. Peak C and peak D may be derived from dead cells and organic matter produced during IOM extraction. Besides, the low response values of peaks C and D indicate that the ultrasonic fracture extraction method has less effect on IOM.

3.3.7. Zeta potential

Since *M. aeruginosa* cells are in the form of stable colloids in aqueous solution, the stability reduces as the electrical charge on the surface of algal cells declines, forming aggregates that settle out of suspension [54]. The change in the zeta potential of the algae after treatment by Ag/AgCl@ZIF-8 coating is illustrated in Fig. 11. The zeta potential value of the control sample contributed no significant change at the end of the photocatalytic degradation. However, the absolute zeta value in the treated sample increased slightly with the initial value at 48 mV and then reduced significantly. The increase of zeta value in the early stage of treatment was mainly due to negative charges released from a large amount of dissolved organic matter (DOM). DOM has an anionic character, which makes *M. aeruginosa* cells negatively charged. The subsequent decrease may occur because the cell membrane was further damaged and DOM was degraded by ROS, reducing the electrical charge on the surface of algal cells. Hence, the above results show that algal cells can be broken and aggregated under visible light induced by

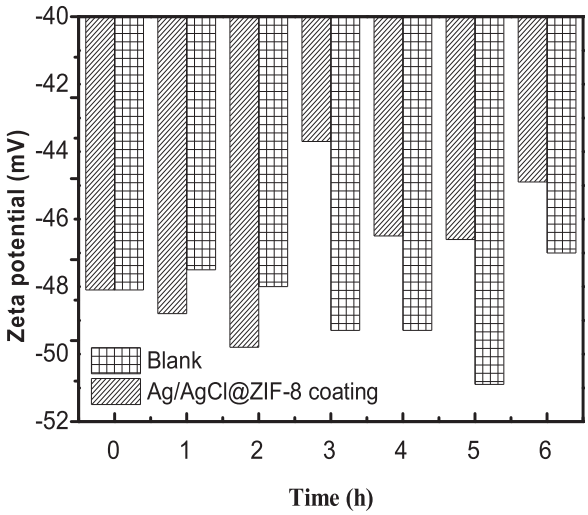

Fig. 11. Changes of Zeta potential in algae solution during photocatalytic inactivation of *M. aeruginosa* by Ag/AgCl@ZIF-8 coating.

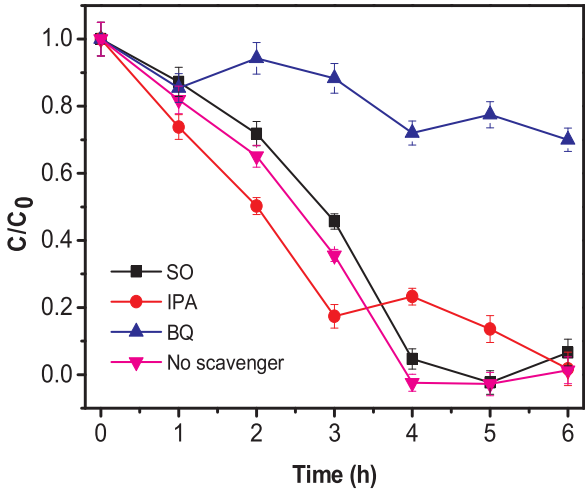

Fig. 12. Photocatalytic inactivation of *M. aeruginosa* in the presence of different scavengers (C_0 = 2.74 mg/L, pH = 7.0, IPA = 1 mM, BQ = 1 mM, SO = 1 mM).

Ag/AgCl@ZIF-8 coating. Besides, algal removal efficiency is presumably enhanced by aggregation effect [55].

3.4. Mechanism of MOF coating inhibiting the growth of algal cells

Reactive oxygen species quenching experiments are conducted to reveal the mechanism of the photocatalytic process. Fig. 12. demonstrates the effects of different scavengers on the degradation efficiency of *M. aeruginosa* under visible light. The residual content of chlorophyll *a* was almost completely degraded with no scavenger added when the duration of photocatalytic treatment was prolonged from 0 h to 4 h. It is clear that the algae removal rate was distinctively inhibited by the $O_2{\cdot}^-$ scavenger when BQ was added. The removal rate of chlorophyll *a* was less than 30% after 6 h of treatment, which identified that $O_2{\cdot}^-$ was the primary reactive species. The algae removal trend under visible light conforms to the control group with the addition of SO, which decreased at a lower rate than that of the untreated group and attributed no significant inhibition of chlorophyll *a*. The presence of IPA inhibited the reaction to some extent, indicating that ·OH was also involved in the photocatalytic algae removal process. In summary, the contribution of the three reactive oxygen species is $O_2{\cdot}^- > h^+ >$ ·OH.

To further elucidate the changes of functional groups on the surface of algal cells, FTIR was performed since ROSs produced by MOF coating could interact with macromolecules on the cell membrane (e.g., proteins, lipids, carbohydrates). The peak intensities reduce in the treated group, while in the control group, there was no significant decline compared with the initial intensities (Fig. 13a). The characteristic peaks of functional groups in the surface of *M. aeruginosa* cells gradually decreased as the treatment time was prolonged to 6 h (Fig. 13b). The peaks at 1024 cm^{-1} and 1078 cm^{-1} almost disappeared after 2 h, indicating that the lipid molecule of the algal cells was severely damaged by oxidation [56]. The vibrational absorption peaks at 1540 cm^{-1} and 1640 cm^{-1} related to the stretching vibration of C—N and C═O, respectively. The decrease of intensity in peaks 1540 cm^{-1} and 1640 cm^{-1} suggests that the hydrophilic terminal of amines on the outer phospholipid bilayers was destroyed. The vibrational absorption peaks at 3000 cm^{-1} and 2865 cm^{-1} were due to the stretching vibration of C—N heterocycles. The decline of peaks 3000 cm^{-1} and 2865 cm^{-1} implies that two aliphatic chains of the lipid molecule on the epidermis of algal cells were also damaged. Hence, the functional groups of *M. aeruginosa* cell wall and membrane were degraded into small molecules or inorganic substances by peroxidation induced by Ag/AgCl@ZIF-8 coating, thus inactivating of the growth of algal cells.

Based on the above results, a possible photocatalytic mechanism for

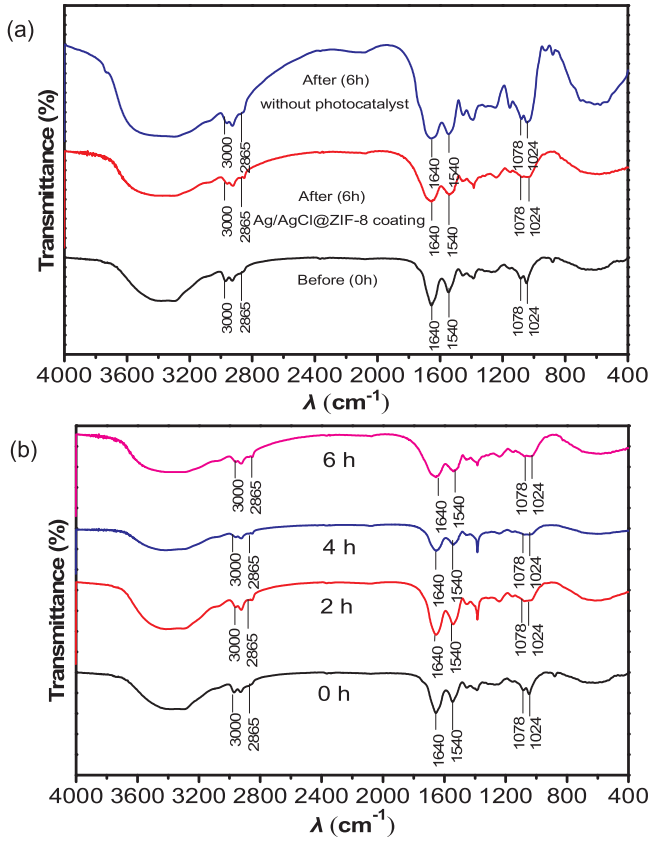

Fig. 13. FTIR spectra of algae cells (a) before and after photocatalytic inactivation, (b) during the experimental process by Ag/AgCl@ZIF-8 coating.

the degradation of *M. aeruginosa* induced by Ag/AgCl@ZIF-8 coating under visible light is proposed (Scheme 1). According to our previous study, Ag/AgCl can be inspired by visible light to form h^+ and e^- for its narrow energy band, and then e- delivered by heterojunction (Ag^0) to ZIF-8 surface could reduce O_2 which adsorbed on the surface of materials to O_2·- when the conduction band of the materials is more negative than $O_2/ O_2{\cdot}^-$ (-0.046 eV vs. NHE) [23]. This indicates that $O_2{\cdot}^-$ plays a key role in the photocatalytic inhibition when using Ag/AgCl@ZIF-8 coating, which could irreversibly damage the cell walls and membranes, and lead to electrolyte leakage, pigment bleaching, collapse of antioxidant enzyme system, protein inactivation, and the consequent death of *M. aeruginosa* as ROSs accumulated in the algal cells. Furthermore, lipid molecules on the phospholipid bilayers are degraded by peroxidation during the inhibition treatment. As a result, the Ag/AgCl@ZIF-8 coating can be applied as an efficiency photocatalyst under visible light for the inactivation of harmful cyanobacteria.

4. Conclusion

As a novel floating photocatalyst, Ag/AgCl@ZIF-8 coating has a broad application prospects against the harmful cyanobacteria in eutrophic water bodies. In this study, sponge loaded with Ag/AgCl@ZIF-8 was prepared via a simple dip-coating method. According to the analysis above, it can be concluded that the MOF coating modified with SDS enhanced the load capacity of the carrier and exhibited the outstanding performance of the photocatalytic activity. The attack of ROSs produced under visible light (e.g., $O_2{\cdot}^-$) damaged cells wall and membrane permeability and subsequently increased the oxidation stress, resulting in the destruction of *M. aeruginosa*. Besides, the floating catalyst is of the great importance of the environmental significance since it can prevent secondary pollution induced by powder photocatalyst. In conclusion, we hope the present work will provide a new

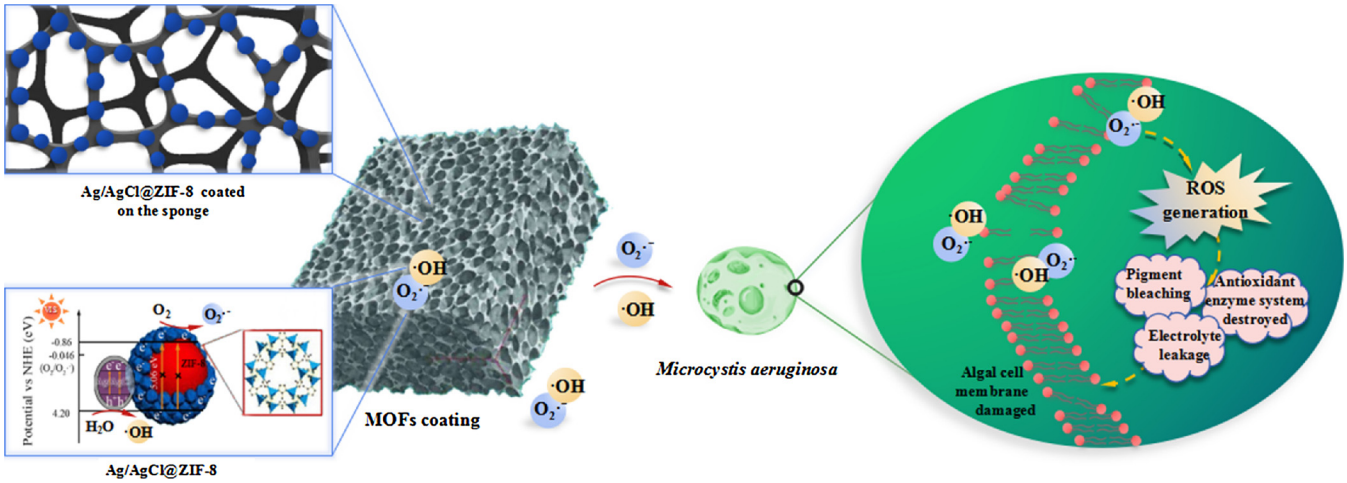

Scheme 1. A possible mechanism for photocatalytic inactivation of *M. aeruginosa* induced by Ag/AgCl@ZIF-8 coating under visible light.

dimension in the removal of harmful cyanobacteria by floating photocatalyst.

Declarations of interest

None.

Acknowledgments

The authors would like to gratefully acknowledge the financially support from the National Natural Science Foundation of China (No. 51778146 and No. 51778082), the Outstanding Youth Fund of Fujian Province in China (No. 2018J06013), the Technical Research Project of Shenzhen Municipal Science and Technology Innovation Commission in China (No. 20170422), and the Open Project Program of National Engineering Research Center for Environmental Photocatalysis (No. NERCEP-201901).

Appendix A. Supplementary data

Supplementary material related to this article can be found, in the online version, at doi:https://doi.org/10.1016/j.apcatb.2019.117866.

References

[1] H.W. Paerl, T.G. Otten, Science 342 (2013) 433–434.
[2] B. Bakheet, M.A. Islam, J. Beardall, X. Zhang, D. McCarthy, Chem. Eng. J. 350 (2018) 616–626.
[3] L. Chen, Y. Sun, W. Sun, K.J. Shah, Y. Xu, H. Zheng, Sep. Purif. Technol. (2019) 10–19.
[4] E.S.M. Shaaban, R.K. Badawy, H.A. Mansour, M.E. Abdel-Rahman, Y.I.E. Aboulsoud, J. Appl. Phycol. 29 (2017) 1–14.
[5] A. Švanys, R. Paškauskas, S. Hilt, Hydrobiologia 737 (2014) 57–66.
[6] G.D. Fan, W. Chen, Z.Y. Su, R.J. Lin, R.X. Xu, X.L. Lin, Q.Z. Zhong, Desalin. Water Treat. (2017) 70–79.
[7] P. Kondzior, A. Butarewicz, J Ecol Eng 19 (2018) 18–28.
[8] M. Vanderstukken, N. Mazzeo, W. Van Colen, S.A.J. Declerck, K. Muylaert, Freshw. Rev. (2011) 1837–1849.
[9] P.A. Reddy, P.V. Reddy, E. Kwon, K.H. Kim, T. Akter, S. Kalagara, Environ. Int. 91 (2016) 94–103.
[10] M. Cho, H. Chung, W. Choi, J. Yoon, Water Res. 38 (2004) 1069–1077.
[11] K. Youngmin, H.H. Min, L. Wang, K. Ikjoon, Y. Yeoheung, L. Hyoyoung, Sci. Rep-UK 6 (2016) 25212.
[12] Y.Z. By Zhang, W.Z. Zhang, Rare Metal. Mat. Eng. (2007) 1299–1303.
[13] E.M. Dias, C. Petit, J Mater Chem A 3 (2015) 22484–22506.
[14] P. Sathe, M.T.Z. Myint, S. Dobretsov, J. Dutta, Sep. Purif. Technol. 162 (2016) 61–67.
[15] W. Wang, G. Li, T. An, D.K.L. Chan, J.C. Yu, P.K. Wong, Appl Catal B-Environ 238 (2018) 126–135.
[16] L. Wang, C. Zhang, F. Gao, G. Mailhot, G. Pan, Chem. Eng. J. 314 (2017) 622–630.
[17] W. Wang, G. Li, D. Xia, T. An, H. Zhao, P.K. Wong, Environ Sci-Nano 4 (2017) 782–799.
[18] S. Ma, S. Zhan, Y. Jia, S. Qiang, Q. Zhou, Appl Catal B-Environ 186 (2016) 77–87.
[19] L. Liu, Z. Liu, H. Bai, D.D. Sun, Water Res. 46 (2012) 1101–1112.
[20] U. Shaislamov, H.J. Lee, Crystengcomm 20 (2018) 7492–7501.
[21] S. Gao, N. Shang, F. Cheng, C. Wang, W. Zhi, RSC Adv. 4 (2014) 39242–39247.
[22] S. Gao, W. Liu, N. Shang, C. Feng, Q. Wu, Z. Wang, C. Wang, RSC Adv. 4 (2014) 61736–61742.
[23] G. Fan, X. Zheng, J. Luo, H. Peng, H. Lin, M. Bao, L. Hong, J. Zhou, Chem. Eng. J. 351 (2018) 782–790.
[24] A. Nel, T. Xia, L. Mädler, N. Li, Science 311 (2006) 622.
[25] J.S. Song, X.W. Wang, J.M. Ma, X.W. Wang, J.W. Wang, J.Z. Zhao, Appl Catal B-Environ (2018) 83–92.
[26] A.G. Slater, A.I. Cooper, Science 348 (2015) 988.
[27] Q.L. Zhu, Q. Xu, Chem. Soc. Rev. 43 (2014) 5468–5512.
[28] S. Zhou, Y. Shao, N. Gao, Y. Deng, L. Li, J. Deng, C. Tan, Water Res. 52 (2014) 199–207.
[29] G. Liu, C. Fan, J. Zhong, L. Zhang, S. Ding, S. Yan, S. Han, Harmful Algae 9 (2010) 413–418.
[30] C. EPA, Methods for Water and Wastewater Analysis, Environmental Science Publishing House of China, Beijing, 2012.
[31] G. Fan, H. Peng, J. Zhang, X. Zheng, G. Zhu, S. Wang, L. Hong, Catal Sci Tech (2018) 5906–5919.
[32] Y. Tao, X. Mao, J. Hu, H.O.L. Mok, L. Wang, D.W.T. Au, J. Zhu, X. Zhang, Chemosphere 93 (2013) 637–644.
[33] Y. Wei, D. Weng, F. Li, X. Zou, D.O. Young, J. Ji, P. Shen, Apoptosis 13 (2008) 1031–1042.
[34] R. Vali Aftari, K. Rezaei, A. Mortazavi, A.R. Bandani, J Food Proces Prese 39 (2016) 3080–3091.
[35] M.P. Padgett, D.W. Krogmann, Photosynth Res 11 (1987) 225–235.
[36] F. Qu, H. Liang, Z. Wang, H. Wang, H. Yu, G. Li, Water Res. 46 (2012) 1490–1500.
[37] J. Tian, C. Wu, H. Yu, S. Gao, G. Li, F. Cui, F. Qu, Water Res. 132 (2018) 190–199.
[38] X. Yang, Z. Wen, Z. Wu, X. Luo, Inorg. Chem. Front. 5 (2018) 687–693.
[39] R. Dong, B. Tian, C. Zeng, T. Li, T. Wang, J. Zhang, J Phys Chem C 117 (2012) 213–220.
[40] K.A. Lin, H. Chang, J. Mater. Chem. A. (2015) 20060–20064.
[41] M. Wen, G. Li, H. Liu, J. Chen, T. An, H. Yamashita, Environ. Sci. Nano (2019) 1006–1025.
[42] P.M. Neumann, Agron. J. 71 (1979) 598–602.
[43] C. Zhang, Y. Yi, K. Hao, G. Liu, G. Wang, Chemosphere 93 (2013) 997–1004.
[44] M. Watanabe, M. Ikeuchi, Photosynth Res 116 (2013) 265–276.
[45] G. Fan, W. Chen, J. Luo, R. Xu, X. Lin, X. Zheng, H. Peng, Desalin. Water Treat. 78 (2017) 350–359.
[46] Z. Wang, D. Li, H. Qin, Y. Li, Environ Pollut 160 (2012) 34–41.
[47] M. Zamocky, P.G. Furtmüller, C. Obinger, Antioxid Redox Sign 10 (2008) 1527–1548.
[48] W. Wanjun, J.C. Yu, X. Dehua, W. Po Keung, L. Yecheng, Environ. Sci. Technol. 47 (2013) 8724–8732.
[49] J. Seppälä, M. Balode, Hydrobiologia 363 (1997) 207–217.
[50] J.A. Korak, E.C. Wert, F.L. Rosario-Ortiz, Water Res. 68 (2015) 432–443.
[51] W. Chen, P. Westerhoff, J.A. Leenheer, K. Booksh, Environ. Sci. Technol. 37 (2015) 5701–5710.
[52] H. Xu, H. Pei, H. Xiao, X. Li, C. Ma, W. Hu, J. Photochem. Photobiol. B, Biol. 158 (2016) 23–29.
[53] H.W.H. Wang, D.L.D. Liu, P.W.P. Wang, F.C.F. Cui, Environ Technol Res Util II (2014) 163–166.
[54] P. Li, Y. Song, S. Yu, Water Res. 62 (2014) 241–248.
[55] S.H. Roh, D.H. Kwak, H.J. Jung, K.J. Hwang, I.H. Baek, Y.N. Chun, S.I. Kim, J.W. Lee, Sep. Sci. Technol. (2008) 113–131.
[56] G. Fan, M. Bao, X. Zheng, L. Hong, J. Zhan, Z. Chen, F. Qu, J. Hazard. Mater. 367 (2019) 529–538.